RECENT ADVANCES IN THE MEASUREMENT OF PORE VOLUME COMPRESSIBILITY OF RESERVOIR ROCKS

Shameem Siddiqui*, James J. Funk, Aon A. Khamees and Ahmad M. Al-Harbi
Saudi Aramco R&D Center, Dhahran, KSA
*Now at Texas Tech University, Lubbock, TX, USA

This paper was prepared for presentation at the International Symposium of the Society of Core Analysts held in Abu Dhabi, UAE 29 October-2 November, 2008

ABSTRACT

The compressibility of a reservoir at different pressures is an important parameter affecting reserve forecasts and field development strategies. Among the four definitions proposed by Zimmerman (1991, 2000), the pore volume compressibility, C_{pc} affects the reservoir engineering calculations the most, as it serves as a major energy source for reservoirs. The most commonly-used technique involves using liquid-saturated core plugs connected to a laboratory setup which controls the confining pressure and the pore pressure, and monitors the fluid volume changes in order to derive an average value of C_{pc}. Computerized Tomography (CT) scanners have been used by the petroleum industry for calculating among others, the porosity of core plugs. The changes in the X-ray attenuation coefficient as a function of pressure at different slice locations can be used to calculate the pore volume compressibility. This paper presents a fast new technique involving dual-energy CT-scanning in order to determine the pore volume compressibility. Several tests were conducted on actual core plugs taken from a Middle-Eastern carbonate reservoir and results were compared against those from conventional pore volume compressibility measurements on the same plugs and they matched very well within the range of repeatability of such tests. The results also matched published results (Hariri et al., 1995) on cores taken from the same reservoir. Some of the advantages of the CT-based technique are also discussed in the paper which include the generation of multiple C_{pc} curves, each at a different slice location, the 'visualization' of the changes, the possibility of using either hydrostatic or triaxial cells to make the test more case specific, the possibility of measuring permeability under different stress conditions before, during and after the test and the possibility of observing the failure of the rock under stress if there is a mechanical failure.

INTRODUCTION

Compressibility of a rock is defined as a change in volumetric strain due to change in applied pressure. In other words,

$$c = -\frac{1}{V_i}\frac{\partial V}{\partial p} \quad \text{.....} \quad (1)$$

Where, c is the compressibility (in psi^{-1}), V is the volume of reservoir rock (in cm^3), P is the pressure (in psi) and i is the subscript denoting the initial condition. Solids have only one compressibility - the bulk volume compressibility. Since rocks are porous and there are

two independent volumes - the bulk volume and the pore volume; and there are two pressures, the confining pressure and the pore pressure (both of these pressures can be varied independently), there can be four different compressibilities through the stress-strain relations. Zimmerman (1991, 2000) used double subscripts (first one identifying whether the compressibility is for bulk or pore volume, and the second one identifying the pressure that is varied) to denote the following two bulk compressibilities and two pore compressibilities: 1) Bulk Compressibility at Constant Confining Pressure, C_{bp}; 2) Bulk Compressibility at Constant Pore Pressure, C_{bc}; 3)Pore Compressibility at Constant Confining Pressure, C_{pp}; and 4) Pore Compressibility at Constant Pore Pressure, C_{pc}. Out of these four compressibilities, the focus of this paper will only be on the determination of C_{pc} (given by Equation 2), which is the pore volume compressibility at constant pore pressure.

$$C_{pc} = -\frac{1}{V_p}\left[\frac{\partial V_p}{\partial p_p}\right]_{pp} \quad \text{.....2}$$

The standard test for C_{pc} is a hydrostatic test in which a fluid saturated rock of known initial pore volume is put inside a coreholder at a constant pore pressure (typically atmospheric). The confining pressure is then slowly increased in stages and the volume of fluid expelled from the pores is measured (typically with an LVDT attached to the pore pressure intensifier piston). A commercial pore volume compressibility measurement device, marketed under the name Autolab (by New England Research), is used commonly for C_{pc} measurement in the lab..

The compressibility (C_{pc}) is usually determined by taking the slope (m) of the logarithmic curve that fits the plot of the pore volume (initial pore volume minus the expelled fluid volume) versus the log of the effective pressure or the net overburden pressure, P_E (difference between the confining pressure, P_c and the pore pressure, P_p, assuming Biot's constant=1). This usually has the form,

$$V_p = m\log(P_E) + c \quad \text{.....3}$$

Then, taking partial derivatives with respect to P_E, we can get

$$\frac{\partial V_p}{\partial P_E} = m\frac{\partial(\log P_E)}{\partial P_E} = m\frac{1}{P_E} \quad \text{.....4}$$

Multiplying both sides by $(\frac{-1}{V_{Pi}})$, we can get

$$\frac{-1}{V_{P_i}}\left[\frac{\partial V_p}{\partial P_E}\right] = \frac{1}{V_{P_i}}\left[\frac{-m}{P_E}\right] \quad \text{.....5}$$

The term on the left of Equation 5 is equal to C_{pc} at constant pore pressure and therefore, the C_{pc} versus P_E plots can be generated for each test.

$$C_{PC} = \frac{1}{V_{P_i}}\left[\frac{-m}{P_E}\right] \quad \text{.....6}$$

Computerized Tomography (CT) scanners have been used in the petroleum industry since the mid '80s for non-destructive evaluation of reservoir rocks and for visualizing and quantifying fluid flow in porous media. Reviews of the various applications of CT in the petroleum industry can be found in the literature [Wellington and Vinegar, 1987; Kantzas, 1990; Akin and Kovscek, 2001; and Withjack et al., 2003]. Recently micro-CT scanners are becoming more popular especially in the areas of pore network modeling [Knackstedt et al., 2004; Youssef et al., 2007] and fracture detection and characterization [Karpyn et al., 2003]. The CT-scanner is capable of measuring one property, the linear attenuation coefficient, μ. The linear attenuation coefficient is given by the Beer's law and it is mainly a function of the density and the effective number of the object which is being scanned by the X-ray CT-scanner. For simplicity, the medical industry uses an internationally standardized scale called the CT number, *CTN* (in Housfield Units, HU), for describing the CT attenuation data. The unit is based on setting the *CTN* of air at -1000 HU and the *CTN* for water at 0 HU.

Although both CT and micro-CT have been used extensively for multiphase fluid flow studies and to some extent, for qualitative and quantitative (mainly density and porosity determination) characterization of rocks, to this date there is very few published work on the use of CT techniques to determine the mechanical properties, especially pore volume compressibility of reservoir rocks. Being a powerful porosity tool, CT shows a strong potential for being used in the determination of pore volume compressibility. Wellington and Vinegar [1987] measured bulk and uniaxial compressibility on a small Castlegate sandstone by using CT-derived normalized density changes as a function of normalized axial stresses. They subjected the sample to the hydrostatic loading of 1000 psi in an aluminum compaction cell, followed by uniaxial compaction until failure and used the stress-strain information to calculate the bulk compressibility and Poisson's ratio. Karacan et al. [2001], using CT-scanners, evaluated porosity change and rock failure as a function of confining pressure and end load with Cordova limestone and Berea sandstone cores placed inside a tri-axial cell. They did not calculate any pore volume compressibility in this study although they observed large porosity and permeability reductions due to the applied stress.

EXPERIMENTAL SETUP

This experimental setup (see Figure 1) is modified from a typical CT coreflooding setup designed for visualization of the simultaneous motion of oil and water inside cores [Siddiqui et al., 2000]. It mainly consists of an HD-350 petrophysical CT-scanner, two Quizix positive displacement pumps, a CT coreholder, a vacuum pump, an electronic balance, a pressure transducer with data acquisition system, valves and stainless steel or

PEEK tubing. The specially-designed CT coreholder (Temco FCH series, rated at 5000 psi and 200 °C, with Viton sleeve for 1-1/2" diameter and up to 12" long cores) guarantees very low X-ray attenuation while providing sufficient strength. The coreholder used is a hydrostatic coreholder with one fixed and one floating end plug.

The experimental setup shown in Figure 1 was designed to operate at room temperatures. For conducting experiments at high temperatures, a recirculating heating system was also used for one of the experiments described in this paper. Since an oven cannot be installed around the scanner or even the coreholder, the heating must be provided indirectly by flowing hot fluids (water or ethylene glycol-water mix) through the annular space between the inner wall of the coreholder and the outside of the rubber sleeve. The fluids to be injected through the core are kept inside the oven in floating piston accumulators from where they are lead to the inlet end of the coreholder through insulated stainless steel lines.

Prior to conducting the tests, the CT-scanner needed to be calibrated for generating artifact-free images of the core plugs inside the coreholder. Two separate calibration tables for 140 kV-100 mA and 80 kV-200 mA were prepared in advance following manufacturer's instructions. In order to switch from one power setting to another, the appropriate calibration table was pulled up rather than just setting the parameters on the control panel of the scanner. Image processing was mainly conducted using a petrophysical image processing package (VoxelCalc by KehlCo), with powerful routines for region-of-interest (ROI) statistics, image subtraction, dual-energy based density-atomic number calculation, and exporting files for display using a variety of 3-D visualization programs.

EXPERIMENTAL PROCEDURE

For the determination of C_{pc}, with hydrostatic compaction under constant pore pressure using the dual-energy scan-based technique, the following steps are followed:

1. Select a dry core plug, measure its weight, length, diameter, and grain density (using a helium porosimeter). Calculate bulk volume, pore volume and porosity.
2. Mount the core plug inside a CT coreholder and apply some initial confining pressure (typically 200 to 500 psi), enough to make a good seal between the rubber sleeve and the steel end plugs. Place and secure the coreholder on the scanning table. Take a pilot-scan (digital radiograph) to locate the starting slice position and number of slices needed to cover the core plug using about 5-mm thick X-ray beams.
3. Place the balance and a brine-filled (containing 20% by weight sodium iodide, NaI) plastic bottle and connect a nylon tubing to the inlet manifold. Pull vacuum on the core from the outlet side (200-300 μ-torr preferred). While pulling vacuum, bring up the high-energy calibration table and activate it. Take a scan of the core plug under vacuum at several slice locations for full coverage at the high-energy setting (typically at 140 kV, 100 mA, with 5 mm thickness and 5 mm scan interval). Bring up the low-energy calibration table and activate it by rebooting. Take a scan of the

core plug under vacuum at the same slice locations for full coverage at the low-energy setting (typically at 80 kV, 200 mA, with 5 mm thickness and 5 mm scan interval).

4. Open the inlet valve to saturate the core with the brine until brine is seen at the outlet end of the core plug. Close the outlet valve and stop the vacuum pump. Record the total volume injected and compare against the volume measured in Step 1. The two volumes should be very close if the dead volumes are taken into account.

5. Move the flexible tubing and the plastic bottle on the balance to the outlet end of the core and connect to the outlet line. Connect a line from the brine injection pump to the core inlet, connect the core outlet to a back-pressure regulator set at pressure 100 psi below the initial confining pressure, open the core outlet valve and flow through the core with 20% by weight NaI brine, for several pore volumes (PV) to completely saturate the core. This is a very important step for overall material balance. Measure the brine permeability of the sample for future reference.

6. Stop the pump, close the inlet valve but leave the outlet valve open. Scan at low- and high-energy settings for getting the data for the saturated core at the initial conditions (change the calibration tables as needed).

7. Slowly start increasing the confining pressure to the first value (e.g. 1000 psig). Use the pump's safety settings not to exceed that pressure. Wait about ten minutes or more for the system to come to equilibrium or until the weight at the balance shows no change). Scan the core at high- and low-energy settings for that confining pressure. Repeat the above step until the highest confining pressure is reached (e.g. for 2000, 3000, 4000 and 4500 psig).

8. Flow brine through the core at the highest pressure to calculate the permeability under stressed condition, if needed.

9. Slowly release some pressure to the next lower confining pressure setting (use Quizix pump's constant pressure intake option, if available). Pump some brine through the core (about 1 PV) to replenish its pore space. Scan the core at high- and low-energy settings at the same slice locations as before.

10. Repeat the above step until the initial confining pressure is reached. Flow brine through the core to calculate the permeability at initial conditions after the test.

11. For tests conducted at higher temperatures keep the brine in a floating piston accumulator inside the oven and use insulated lines from the accumulator to the core inlet. Use the positive displacement pump of the recirculating heating system for applying confining pressure and temperature.

12. Dismantle the coreholder to take the core plug out. Clean and dry the inside of the coreholder and put the dual-energy calibration 'standards' (cylinder of homogeneous materials having the same diameter as the core plugs) such as Quartz, Aluminum, Poly Vinyl Chloride, Teflon, Polyethylene, Kel-F, Macor, etc. inside

the coreholder and scan them at the high- and low-energy settings. Also scan the brine and air inside the coreholder at the two energies.

For CT-scanners not set up to do dual-energy scanning, only scanning at the highest energy (e.g. 140 kV) is recommended. For this case the grain density data (using a helium porosimeter or equivalent) for the core plug must be collected prior to CT scanning. Since grain density varies from slice to slice, using an average value may not always accurately represent the inherent heterogeneities of the rock sample in this case.

DATA ANALYSIS

The dual-energy based CT-scanning procedure has been described by Wellington and Vinegar [1987] and by Siddiqui and Khamees [2004]. Through the use of appropriate calibration 'standards' (at least three required) with a pair of CT-scan images taken at the high-energy setting (where Compton Scattering dominates) and low-energy setting (where Photoelectric Factor dominates), one can generate the effective atomic number (Z_{eff}) and bulk density (ρ_b) of a rock sample. The petrophysical CT image processing software, Voxelcalc was used for generating the density and effective atomic number images and quantitative data for this paper although it is possible to generate just the density and atomic number data (based on average slice values) using the calculation procedure shown by Siddiqui and Khamees [2004]. During image data processing, a circular region-of-interest (ROI), slightly smaller than the circle representing the core plug (to eliminate the boundary effects [Unalmiser and Stewart, 1989] and to avoid the rubber sleeve) but large enough to represent most of the rock materials must be used consistently for all the slices for a particular test. Going through the different slices and adjusting the ROI size accordingly before permanently selecting a particular ROI will also ensure good quality data. Once the ROI is selected, the diameter of the circle in terms of pixels should be recorded, which will in turn be used to calculate the circular area in cm^2 and also the bulk volume of each slice in cm^3. Step-by-step calculation procedure for the dual-energy based method is given below.

1. Calculate the grain density using the dual-energy based bulk density and Z_{eff} data. This requires the knowledge of major minerals present in the core. For instance, for the carbonate samples from the Middle-Eastern reservoir used for this study, the major minerals were calcite (ρ_{ma}=2.71g/cm^3, Z_{eff} = 15.7100) and dolomite (ρ_{ma} = 2.87g/cm^3, Z_{eff} =1 3.7438). First, calculate the calcite fraction (f_{calc}) using Equation 15, and then the grain density (ρ_{ma}) using Equation 16.

$$f_{calc} = 0.5086 Z_{eff} - 6.99 \quad \text{.....7}$$

$$\rho_{ma} = f_{calc} * 2.71 + (1 - f_{calc}) * 2.87 \quad \text{..... 8}$$

2. Calculate the initial porosity, ϕ_i, using the standard relationship between the grain density (ρ_{ma}), bulk density (ρ_b) and fluid density (ρ_f), with air as the initial fluid

present in the pores. The initial pore volume, V_{pi} for each slice can be calculated using the bulk volume calculated based on the ROI size..

$$\phi_i = \frac{\rho_{ma} - \rho_b}{\rho_{ma} - \rho_f} \quad \text{..... 9}$$

3. Calculate the apparent pore fluid (brine) density, ρ_{fa} (due to the combined effects of Z_{eff} and density) as a function of the initial brine-filled bulk density, ρ_{bi}, and the initial porosity, ϕ_i, using Equation 10.

$$\rho_{fa} = \frac{\rho_{bi} - (1 - \phi_i)\rho_{ma}}{\phi_i} \quad \text{..... 10}$$

4. Calculate the new porosity, ϕ_{new} and the new pore volume, V_{pnew}, at another pressure stage by using the following equations:

$$\phi_{new} = \frac{\rho_{ma} - \rho_{bnew}}{\rho_{ma} - \rho_{fa}} \quad \text{..... 11}$$

$$V_{pnew} = V_b * \phi_{new} \quad \text{..... 12}$$

Note that the only assumptions used here are, the grain density ρ_{ma}, and the fluid density, ρ_f, do not change at the pressures used in the test. These are both valid assumptions as the grain compressibility is very low and the fluid inside the core is always subject to the same atmospheric pressure. The main difference between the single- and dual-energy based techniques is the way the data are analyzed. For analyzing the single-energy data the grain density must be known or assumed. Basically the steps needed for data analysis involves calculating the ϕ_i and V_{pi} at each slice location, generating a linear relationship between the single-scan *CTN* versus bulk density and using this relationship to calculate density changes taking place within the ROI as different confining pressures are applied.

When stress is applied from all sides on a core sample that is kept in a hydrostatic coreholder, some deformation takes place. If the elastic limit is not exceeded, the sample should return to its original size when stress is removed. This is referred to as a cycle of stress. For the CT-based test for pore volume compressibility, C_{pc} described in this paper, the hydrostatic pressure is the only stress applied and therefore stress and pressure are used synonymously. During the first half cycle of such a test, the pore space is kept at atmospheric conditions and the confining pressure is increased to the maximum pressure. The bulk and pore volumes of the core decreases (density increases) and there is evacuation of some fluid from the pore space. If the test is not designed properly, the change in density can be permanent. Within this volume of interest it is possible to account for the change in pore volume of the core by a change in density during every stage of applied pressure by taking scans at the same location. By taking a number of volumes of interest at every slice location, it is possible to evaluate the pore volume change in the entire core during both the half cycles of a pore volume compressibility test.

Once the pore volumes are known as a function of the net confining pressure, P_E (applied confining pressure minus the pore pressure), the C_{pc} values can be easily calculated.

RESULTS

CT-assisted pore volume compressibility measurements were conducted on four core plugs from a Middle-Eastern carbonate reservoir. Two of these core plugs were analyzed using the dual-energy technique and two others were analyzed using the single-energy technique. Table 1 shows some of the measured and calculated properties of the four samples.

The first dual-energy based CT experiment to determine C_{pc} was conducted with Sample #34. This plug was previously tested at the rock mechanics lab to 2320 psi (16 Mpa) and it was chosen in order to validate the results generated by the CT-based technique for measuring pore volume compressibility. Figure 3 shows the porosity profile within the core plug #34 at different stages of imposed confining pressures. The porosity gradient discussed above is clearly seen in the data for the initial pressure of 250 psi. Figure 3 shows the calculated pore volumes (V_p) as a function of the net confining pressure. The arithmetic average of the V_p values at each location (known as the ALL dataset) is used for generating the logarithmic fit of the data (first half cycle shown). The data generated by the CT-based technique were compared against the C_{pc} data, which were independently generated using an Autolab-1000 apparatus prior to the CT experiment. Figure 5 shows that the two half cycles of Autolab data are within the same order of magnitude as the data generated by the CT-based technique. Figure 6 shows the band of C_{pc} data generated from this experiment placed against the Autolab-generated C_{pc} data.

The second dual-scan experiment described here was conducted with a core plug referred to as Sample #28. This plug may have been tested using the Autolab system prior to the test (data unavailable) and it was tested again after the test (data available). Again, the dual-scan analysis procedure described above was applied to calculate changes taking place inside the core during the application of different confining pressure values from 200 psi to a maximum of 4500 psi, while keeping the pore pressure at atmospheric. A total of nine 5-mm thick slices were used in the data analysis (representative volume of 4.90 cc each), two other slices at the end were ignored as they contained the effects of the steel end plugs. The data generated by the CT-based technique were compared against the C_{pc} data, which were independently generated using Autolab-1000 after the CT experiment. Figure 7 shows that the second half cycle of Autolab data are almost on top of the data generated by the CT-based technique. The data for the first half cycle, although within the same order of magnitude as the Autolab data for the same half cycle, showed values that are generally less. This may be due to seal conformance issues or a minor leak.

The first single-energy scan test described here was conducted with Plug #9 from the same field as above. Figure 8 shows the C_{pc} vs. P_E for the first and second half cycles and the average of the two cycles, calculated using the single-energy data analysis technique. No rock mechanics data were available for comparing against the data from the test although the curves show the good overall shape (steep slope at lower pressures and gentle slope at

higher pressures) for C_{pc} data similar to the ones discussed above. The overall magnitude of the C_{pc} was generally lower than those for the previously discussed samples, varying merely from about 2.8×10^{-6} to about 0.21×10^{-6} per psi for the pressure range used and this is most likely due to the prior rock-mechanics tests done on the sample. The permeability values at the initial confining pressure of 300 psi was monitored in the experiment with Plug #9 and it showed a reduction of 34.7% reduction after the pore volume compressibility test. Data for Sample #43, used in the second single energy test are not discussed here but it also showed the ability to calculate C_{pc} using the same technique.

The data generated by the single- and dual-energy scan-based techniques for pore volume compressibility determination of the four samples were compared against the published literature on Saudi Arabian carbonate reservoir rocks [Harari et al., 1995]. In their work with 19 carbonate plugs in four groups – Grainstone (GS), Packstone (PS), Wackestone (WS), and Mudstone (MS), Harari et al. [1995] came up with the correlation equations for each carbonate rock group. From their data four plots were generated, one for each group, based on the best coefficient of correlation, and then the data derived from the present work were plotted against them. The results are shown in Figure 9. There is a very good agreement between the two sets of data showing that the data generated by the CT-based PVC calculation procedure are also comparable with published literature values.

CONCLUSIONS

1. A new experimental setup and set of procedures were developed to determine 3-dimensional pore volume compressibility. The CT pore volume compressibility test results were in very good agreement with the conventional tests conducted with the Autolab-1000 system within the limit of repeatability of such tests. These results also compared very well against the published literature values on Saudi Arabian carbonates provided by Harari et al. [1995].
2. Two different data analysis techniques, one each for the single- and dual-energy settings, were developed with detailed operating procedures. Out of the two, the dual-energy scanning-based technique is recommended because it does not require the prior knowledge of grain density.
3. The three-dimensional (CT-based) pore volume compressibility measurement technique discussed in this paper can generate a series of pore volume compressibility data (function of the slice thickness and scan interval) rather than a single value for each core. This translates to one CT-based test being equivalent about 10 tests conducted by a conventional system. Within each slice volume, the effects of the inherent heterogeneities can be captured using this new technique and each core plug can furnish a band of data showing the upper and lower bounds of pore volume compressibility. This type of test can also result in significant cost savings.
4. Although no pore volume compressibility test was conducted up to the pressure causing mechanical failure of the core plug, the ability for CT to observe minor fractures within cores can be very useful in identifying samples that failed mechanically during such a test.

REFERENCES

Akin, S. and Kovscek, A.R.: “Use of Computerized Tomography in Petroleum Engineering Research,” Annual Report of SUPRI TR 127, Stanford University, Stanford, CA, August 2001, pp. 63-83.

Harari, Z., Wang, S-T. and Saner, S.: “Pore Compressibility Study of Arabian Carbonate Reservoir Rocks, SPE Formation Evaluation, December, 1995, pp. 207-214.

Karacan, C.O., Grader, A.S. and Halleck, P.M.: “4-D Mapping of Porosity and Investigation of Permeability Changes in Deforming Porous Medium,” SPE 72379 presented at SPE Eastern Regional Meeting held in Canton, OH, 17-19 October 2001.

Karpyn, Z, Alajmi, A., Parada, C, Grader, A.S. and Halleck, P.M.: “Mapping Fracture Apertures Using Micro-Computed Tomography,” SCA-2003-50, presented at the 2000 SCA Symposium held in Pau, France, September 21 - 24, 2003.

Kantzas, A: "Investigation of Physical Properties of Porous Rocks and Fluid Flow Phenomena in Porous Media Using Computer Assisted Tomography," In Situ, Vol. 14, No. 1, 1990, p. 77.

Knackstedt, M.A. , Arns, C.H. , Limaye, A. , Sakellariou, A., Senden, T.J. , Sheppard, A.P., Sok, R.M., Pinczewski,V.: “Digital core laboratory: Properties of reservoir core derived from 3D images”, SPE 87009 (2004), The Asia pacific conference on Integrated Modelling Kuala Lumpur, Malaysia, 29-30 March, 2004.

Siddiqui, S, Funk, J. and Khamees, A.: "Static and Dynamic Measurements of Reservoir Heterogeneities in Carbonate Reservoirs," SCA paper no. 2000-06, presented at the 2000 SCA Symposium held in Abu Dhabi, UAE, October 18 - 22, 2000.

Siddiqui, S. and Khamees, A.A.: "Dual-Energy CT-Scanning Applications in Rock Characterization,” SPE Paper No. 90520, presented at the 2004 SPE Annual Conference and Exhibition held in Houston, Texas, USA, 26-29 September 2004.

Unalmiser, S. and Stewart, R. W.: “Boundary Effect on Porosity Measurements and Its Resolution by Method and Mathematical Means,” The Log Analyst, March-April, 1989, pp. 85-92.

Wellington, S. L. and Vinegar, H. J.: "X-Ray Computerized Tomography," Journal of Petroleum Technology, August, 1987, p. 885.

Withjack, E.M., Devier, C. and Michael, G.: "The Role of X-Ray Computed Tomography in Core Analysis," SPE paper 83467 presented at the SPE Western Regional/AAPG Pacific Section Joint Meeting held in Long Beach, California, May 19-24, 2003.

Youssef, S., Rosenberg, E., Gland, N, Bekri, S. and Vizika, O.: “Quantitative 3d Characterisation Of The Pore Space Of Real Rocks: Improved μ-CT Resolution and Pore Extraction Methodology,” SCA2007-17, presented at the International Symposium of the Society of Core Analysts Calgary, September 10-12, 2007.

Zimmerman R.W.: Compressibility of Sandstones, Elsevier Publications, New York, 1991, p. 21.

Zimmerman, R.W.: "Implications of static poroelasticity for reservoir compaction," Proceedings of the 4th North American Rock Mechanics Symposium, NARMS 2000, J. Girard et al. (eds.), Balkema, Rotterdam, 2000, pp. 169-172.

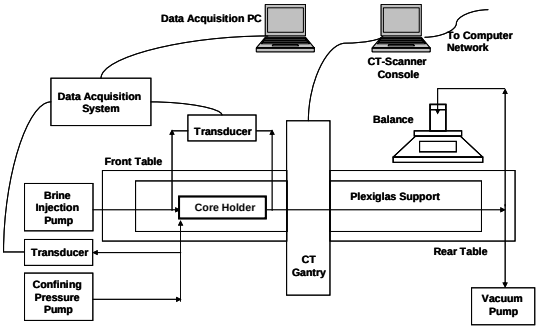

Figure 1: Schematic of the experimental setup

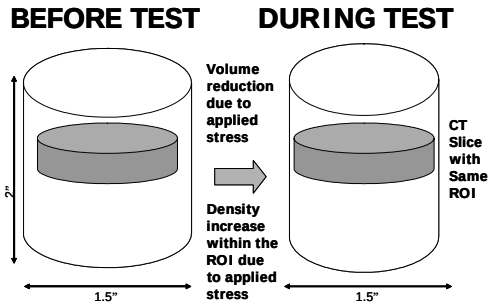

Figure 2: Picture showing how the change in volume during a laboratory pore volume compressibility test relates to the change in density within a fixed region-of-interest (ROI). This forms the basis of calculation.

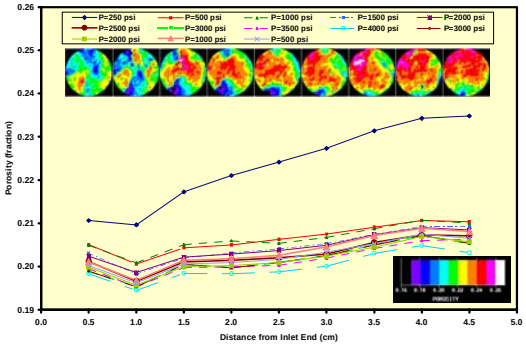

Figure 3: Dual-scan CT generated porosity at each slice location using Sample #34. The insets show porosity distribution within each slice (top) and the color legend (bottom) at the beginning of the test.

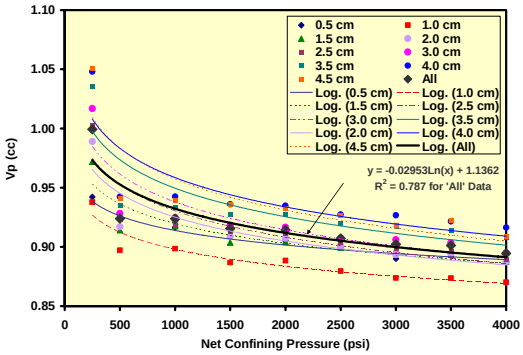

Figure 4: Pore Volume vs. Net Confining Pressure for Sample #34 at different slice locations and the logarithmic fit for the average (shown as ALL) dataset.

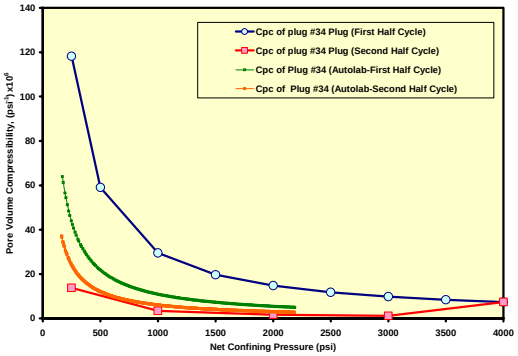

Figure 5: Comparison between the CT-generated and the Autolab-generated Pore Volume Compressibility data for Sample #34 (both half cycles). The Autolab test was run up to 2400 psi prior to the test using CT.

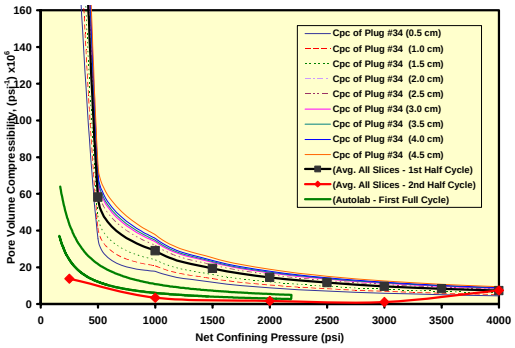

Figure 6: Comparison between the Autolab-generated and the CT-generated Pore Volume Compressibility data (first half cycle for the individual slice location data and both half cycles for the average data).

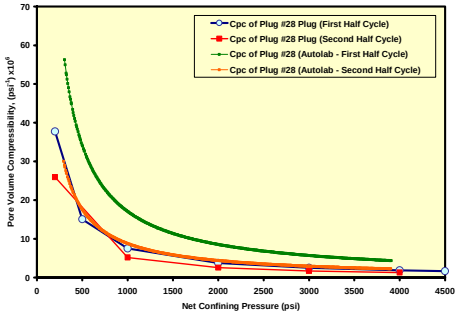

Figure 7: Comparison between the CT-generated and the Autolab-generated Pore Volume Compressibility data for Sample #28 (both half cycles). The Autolab test was run up to 4000 psi after the test using CT.

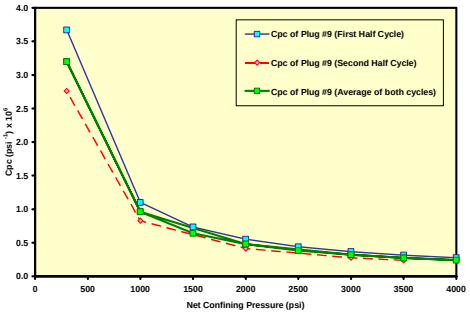

Figure 8: Pore Volume Compressibility vs. Net Confining Pressure for Sample #9 based on the logarithmic fit for the average (ALL) dataset for each of the two half cycles and the individual half cycles.

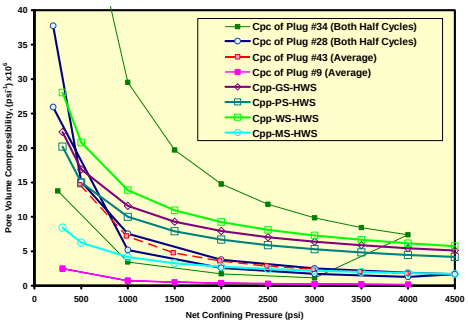

Figure 9: Comparison between the CT-generated (Single- and Dual-Scan) and Harari et al. [1995] correlation data showing a good agreement between CT-generated data and published correlations.

Table 1: Core Plug Properties

Property and Unit	DUAL ENERGY		SINGLE ENERGY	
Sample No.	**34**	**28**	**09**	**43**
Length, cm	4.834	4.986	6.706	3.901
Diameter, cm	3.764	3.764	3.785	3.747
Bulk Volume, cm^3	53.79	55.49	75.43	43.01
Dry Weight, g	109.04	102.03	139.05	81.73
Bulk Density of Dry Sample, g/cm^3	2.03	1.84	1.84	1.90
ROI diameter (pixels) and image size	108 and 160	226 and 80	218 and 80	76 and 240
Diameter of Region-of-interest, cm	3.375	3.531	3.406	3.563
Area of Slice, cm^2	8.946	9.794	9.113	9.968
Bulk Volume of Each Slice, cm^3	4.4731	4.8969	4.5563	1.9389
No. of slices used	9	9	12	16
Total Volume, cm^3	40.2578	44.0717	54.6756	31.0224
NaI conc. in brine (by wt)	20%	20%	20%	10%
Routine grain density, g/cm^3	Not measured	Not measured	2.68	2.69
Routine porosity	0.2399	0.3166	0.2928	0.3179
Initial and highest test Pressures, psi	250 & 4000	200 and 4500	300 and 4000	500 and 4000